Supplementary Material

Structure and electronic properties of MoSe$_2$/PtS$_2$ van der Waals heterostructure

Hui Zhang[1], Meng Pei[2], Boyang Liu[1], Zongli Wang[1, *], Xu Zhao[2, *]

*1 Department of Physics, Zhejiang University, Hangzhou 310027, China*

2 School of Physics, Henan Normal University, Xinxiang, Henan 453007, China

The two-step method for optimization

For the step one, to obtain the equilibrium interlayer distance d_0, the binding energy is calculated as a function of the interlayer distance. After fitting the data by the well-known Buckingham potential equation, we will get the equilibrium interlayer distance d_0. For the step two, the MoSe$_2$/PtS$_2$ van der Waals heterostructure with the equilibrium interlayer distance d_0 is constructed and then we perform a full geometric optimization process to obtain the final equilibrium structure.
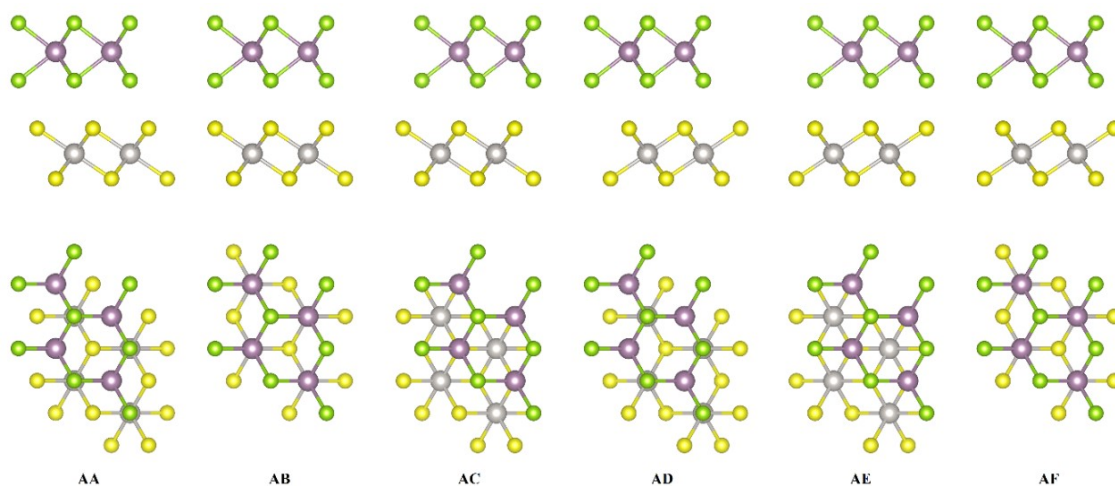
Figure S1. The top and side views of MoSe$_2$/PtS$_2$ van der Waals heterostructures with six different stacking patterns after geometric optimization. The yellow, gray, purple and green balls represent S, Pt, Mo and Se atoms, respectively. In the AA, AB and AC stacking patterns, the Se atoms are on the top of the Pt atoms, the upper S atoms and the lower S atoms, respectively. After rotating the PtS$_2$ layer by 180°, the Se atoms are aligned with the Pt atoms, the upper S atoms and the lower S atoms, respectively, corresponding to the AE, AD and AF stacking patterns.
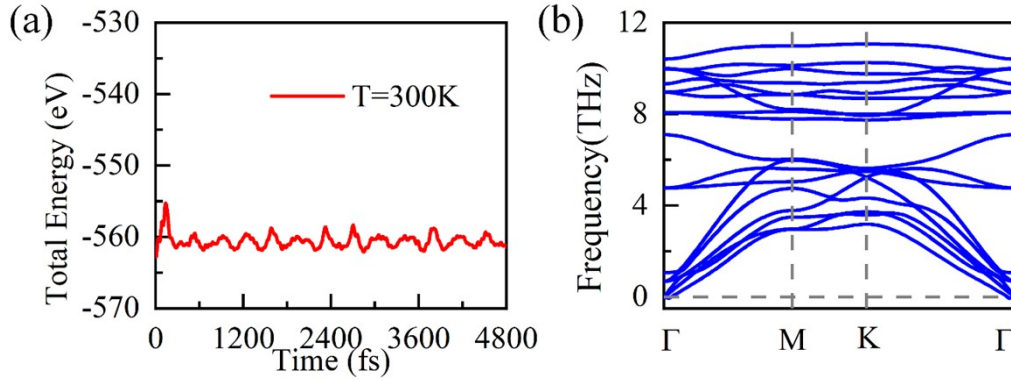
Figure S2. (a) The total energy of $MoSe_2/PtS_2$ heterostructure as a function of the time under the molecular dynamics simulations at room temperature. (b) The phonon dispersion curve of the $MoSe_2/PtS_2$ heterostructure.

In order to further estimate the stability of $MoSe_2/PtS_2$ heterostructure, the ab initio molecular dynamics (AIMD) simulation at room temperature and the phonon spectrum are calculated, as displayed in Fig. S2(a) and Fig. S2(b). Although there is a very small imaginary frequency (-0.05 THz) in the phonon dispersion curve, the imaginary frequency is so small that depositing the $MoSe_2/PtS_2$ heterostructure onto a proper substrate or applying small strain could eliminate it. Moreover, the evolution of total energy with time is fluctuating in a narrow window and the atoms only vibrated slightly around their equilibrium positions, indicating the high thermal stability of the $MoSe_2/PtS_2$ heterostructure. Hence, the $MoSe_2/PtS_2$ heterostructure with the AC staking pattern possess great stability from the views of both the lattice dynamics and thermodynamics, which verifies feasibility to construct the $MoSe_2/PtS_2$ heterostructures in experiments.
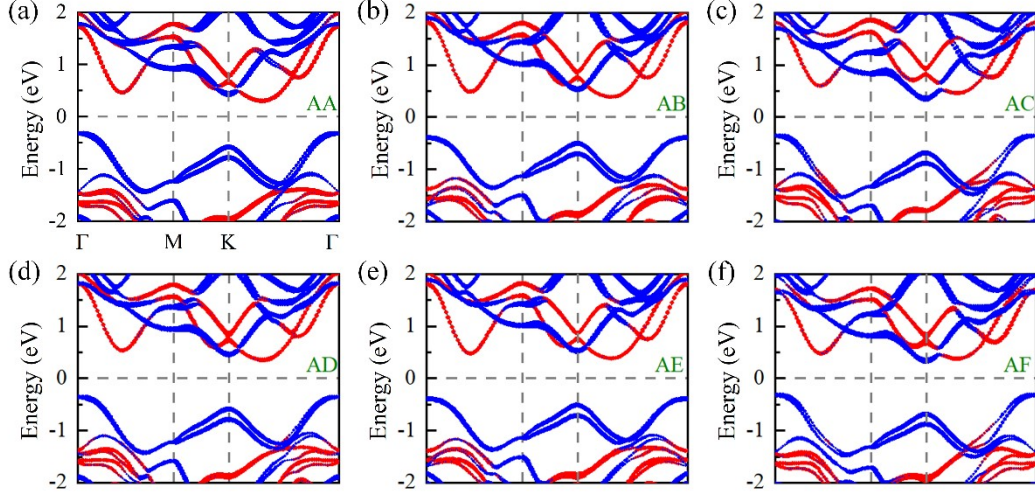
Figure S3. The projected band structures of MoSe$_2$/PtS$_2$ vdWHs with different stacking patterns of (a) AA, (b) AB, (c) AC, (d) AD, (e) AE, and (f) AF, respectively. The blue and red lines represent the contributions from MoSe$_2$ and PtS$_2$ monolayer, respectively. The Fermi level indicated by the black dashed lines is set at zero.

Fig. S3 show projected band structures of the MoSe$_2$/PtS$_2$ heterostructures with different stacking patterns. Obviously, the MoSe$_2$/PtS$_2$ heterostructures with different stacking patterns are indirect band gap semiconductors. The calculated band gaps are 0.612 eV, 0.778 eV, 0.695 eV, 0.699 eV, 0.769 eV, and 0.640 eV for AA, AB, AC, AD, AE and AF, respectively. Furthermore, the MoSe$_2$/PtS$_2$ heterostructures with the AC and AF stacking patterns exhibit the type-I band alignment. The MoSe$_2$/PtS$_2$ heterostructures with the AA, AB, AD and AE stacking patterns possess the type-II staggered-gap band alignment. The type-II band alignment can facilitate the spontaneous separation of electron-hole pairs by localizing electrons and holes in different layers, which is beneficial to the applications in photovoltaics, photocatalysis and optoelectronics.

# Structure and electronic properties of the MoSe₂/PtS₂ heterostructure with AC stacking pattern
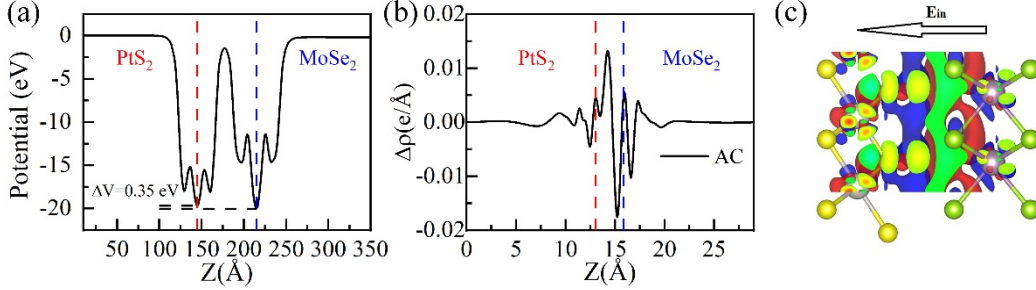
Figure S4. (a) The plane-average electrostatic potential of the MoSe$_2$/PtS$_2$ heterostructure. The vertical dashed red and blue line denotes the PtS$_2$ and MoSe$_2$ layers, respectively. (b) The plane-averaged charge density difference curve of the MoSe$_2$/PtS$_2$ heterostructure (c) The 3D isosurface of the charge density difference for the MoSe$_2$/PtS$_2$ heterostructure. The blue and red areas represent electrons accumulation and depletion, respectively. The isovalue is 0.0001 e/Å^3.

As shown in Fig. S4(a), the MoSe$_2$ layer has deeper potential than that of PtS$_2$ layer. However, the potential difference is only 0.35 eV, which means that there is a weak electronic field across the interface. Thus, the charge transfer between the MoSe$_2$ layer and the PtS$_2$ layer would be small. The Bader charge analysis shows that about 0.014e are transferred from the MoSe$_2$ layer to the PtS$_2$ layer, resulting in the n-doping in PtS$_2$ monolayer and p-doping in MoSe$_2$ monolayer. In order to better understand the process of charge transfer between the MoSe$_2$ and PtS$_2$ layers, the charge density difference (CDD) of MoSe$_2$/PtS$_2$ heterostructure is calculated as follows:

$$\Delta\rho(z) = \iint \rho_{hetero} dxdy - \iint \rho_{MoSe_2} dxdy - \iint \rho_{PtS_2} dxdy ,$$

where ρ_{hetero}, ρ_{MoSe_2} and ρ_{PtS_2} are the charge density of the MoSe$_2$/PtS$_2$ heterostructure, the isolated MoSe$_2$, and PtS$_2$ monolayer, respectively. The charge density difference and the corresponding 3D isosurface of the charge density difference for MoSe$_2$/PtS$_2$ heterostructure is displayed in Fig. S4(b) and (c), respectively. Clearly, the charge redistribution mainly occurs near interfacial region of the heterostructure, indicating that the interaction between the MoSe$_2$ and PtS$_2$ layer is the vdWs interaction rather than the covalent bond.
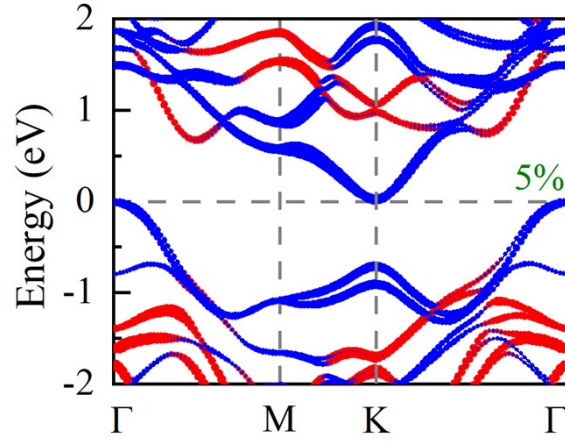
Figure S5. The projected band structures of $MoSe_2/PtS_2$ heterostructure under +5% biaxial tensile strain. The red and blue lines represent the contributions from $MoSe_2$ and PtS_2 monolayer, respectively. The Fermi levels are set to zero. Tensile and compressive biaxial strains are distinguished by the positive and negative signs.
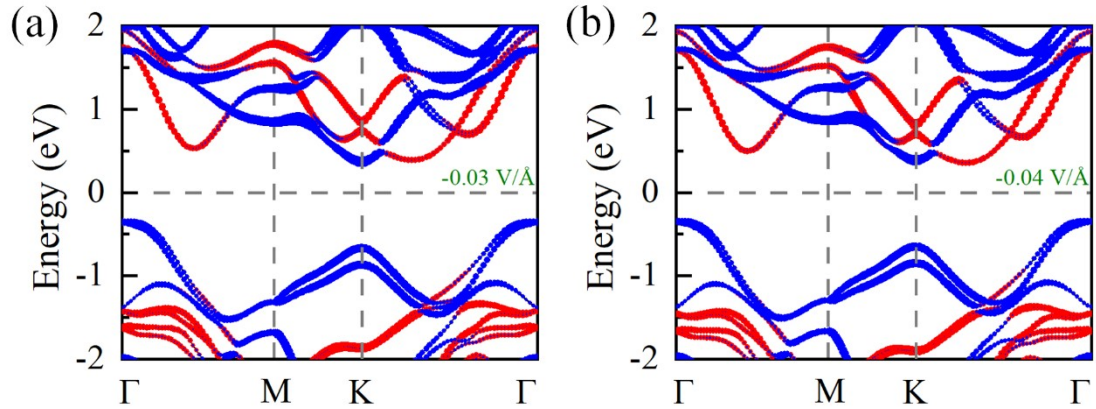
Figure S6. The projected band structures of $MoSe_2/PtS_2$ heterostructure under external electronic field of −0.03 V/Å and −0.04 V/Å. The red and blue lines represent the contributions from $MoSe_2$ and PtS_2 monolayer, respectively. The Fermi levels are set to zero. Tensile and compressive biaxial strains are distinguished by the positive and negative signs.